JOURNAL OF AIRCRAFT
Vol. 30, No. 5, Sept.–Oct. 1993

Unsteady Pressure and Load Measurements on an F/A-18 Vertical Fin

B. H. K. Lee* and F. C. Tang†
Institute for Aerospace Research, Ottawa, Ontario, Canada

Tail buffet on a rigid 6% scale model of the F/A-18 was investigated in the Institute for Aerospace Research 1.5 m trisonic blowdown wind tunnel. Strain gauges were installed on the port fin to measure normal force, root bending and torsion moments. The starboard fin was instrumented with 24 fast-response transducers on each surface for unsteady pressure measurements. Static tests at constant angle of attack were performed to compare the loads and moments from the strain-gauged fin with those determined from pressure measurements. Pitch oscillations of the model were carried out at low frequencies. The mean angle of attack, amplitude of oscillation, and Mach number were varied to note the effects of delay in LEX vortex burst on the vertical fin buffet loads. The envelopes of the unsteady force and pressure signals, rms variations with angle of attack, and probability densities were evaluated to study the characteristics of the normal force and pressures fluctuations on the vertical fin.

Nomenclature

A_j = area of jth panel on vertical fin
BM = vertical fin bending moment
C_B = bending moment coefficient, $BM/qS\bar{c}_f$
C_N = vertical fin normal force coefficient, NF/qS
C'_N = rms value of normal force coefficient
C_p = pressure coefficient
C'_p = rms value of pressure coefficient, p_{rms}/q
C_T = torsion moment coefficient, $TM/qS\bar{c}_f$
$\bar{c}$ = wing mean aerodynamic chord, 210.56 mm
$\bar{c}_f$ = vertical fin mean aerodynamic chord, 127.76 mm
f = frequency
k = nondimensional frequency, $f\bar{c}/U_\infty$
M = freestream Mach number
NF = vertical fin normal force
p_I = pressure on vertical fin inboard surface
p_o = pressure on vertical fin outboard surface
p_{rms} = rms value of pressure
q = freestream dynamic pressure
$R_{e\bar{c}}$ = Reynolds number based on $\bar{c}$
S = surface area of vertical fin, 1.716×10^{-2} m^2
TM = vertical fin torsion moment about $\frac{1}{4}$ chord
U_∞ = freestream velocity
α = angle of attack
α_a = amplitude
α_0 = mean angle of attack
σ = rms value
ϕ = phase angle

I. Introduction

MANEUVERABILITY of high-performance aircraft at large angles of attack is often severely limited by fatique problems associated with tail buffeting. This is especially common for twin-tail aircraft with a leading-edge extension (LEX) such as the F/A-18.

Received March 19, 1992, presented as Paper 92-2675 at the AIAA 10th Applied Aerodynamics Conference, Palo Alto, CA, June 22–24, 1992; revision received June 24, 1992; accepted for publication June 26, 1992.

*Senior Research Officer, National Research Council, High Speed Aerodynamics Laboratory. Associate Fellow AIAA.
†Associate Research Officer, National Research Council, High Speed Aerodynamics Laboratory.

A number of investigations[1–4] have described the characteristics of the LEX vortices and their effects on tail buffet. At the Institute for Aerospace Research (IAR), an investigation of the aerodynamics and tail buffet on a rigid 6% scale model of the F/A-18 at high angle of attack was made in the transonic test section of the 1.5-m trisonic blowdown wind tunnel. The study has been reported in a number of papers which discussed the LEX and fin pressures fluctuations,[5,6] the flowfield behind the vertical fin,[7] and the peak buffet loads experienced by the vertical fin.[8] These investigations illustrate the flow phenomena and provide information on the correlation of the pressure field near the vertical fin with that on the fin itself.

Two wind-tunnel tests were performed. In phase I, measurements of the vertical tail buffet loads were made on the starboard fin with the aid of 48 fast-response transducers arranged in opposing pairs at 24 locations on the inboard and outboard surfaces. An estimate of the loads on the fin was obtained by summing the product of the pressure difference of a pair of transducers across the fin and the area ascribed to that transducer pair.[5] The pressures at all points on a panel were assumed to be in phase and equal to that measured by the transducer. In phase II of the F/A-18 high-alpha studies, the port fin was instrumented with strain gauges to provide accurate measurements of the normal force, root bending, and torsion moments. The data were used to assess the accuracy of the loads and moments derived from pressure measurements.

Some experiments were also conducted to investigate the pressures and loads experienced on the vertical fin with the model performing sinusoidal pitch oscillations at various mean angles of attack, amplitude, Mach number, and frequency. Water-tunnel investigations of the vortex flow pattern[9] show a delay in the bursting of the LEX vortices during pitching motions of the F/A-18. This article shows the lag effect of vortex burst during pitch oscillations on tail buffet loads. Only very low frequencies were investigated since the sting support system in the IAR tunnel is limited to a maximum pitch rate of 15 deg per second.

II. Model and Instrumentation

A. Model and Installation

The model used was a rigid 6% scale of the F/A-18,[5] sting-mounted from a vertically translating strut. A linkage mechanism controlled a pitch angle change from −11 to 22 deg. For these measurements the model was supported on an offset

sting (11-deg crank angle) which gave a model incidence range from 0 to 33 deg. Sting bending under aerodynamic loads resulted in approximately a 2-deg increment pitch angle for the Mach number range tested.

In this article, only results with the LEX fence on are discussed. The leading- and trailing-edge flaps were deflected at 35 and 0 deg. These settings correspond closely to those from flight tests. The stabilator angle was set at −9 deg for this investigation. Through-flow air intakes and flow passages were provided with removable internal chokes. The flow passages terminated in D-shaped exits on each side of the support sting. Models of the AIM 9 missiles were fixed to the wing tips for the measurements.

For static tests, two modes of operation of the tunnel were used. For long runs of 15 s or more, the model was pitched to the preset angle and held constant. This type of run was performed when a sufficiently long record was required for statistical analysis, such as power spectral density or probability density function measurements. For mean or rms values, the pitch-pause mode was used. The number of angles of attack was preprogrammed with a dwell period of typically 2.5–3 s which was sufficient.

Oscillations of the model were limited to a range of very low frequencies. The sting support system was not designed for this mode of operation, but its pitch motion is programmable. In this experiment the sting was programmed to perform sinusoidal motion. The frequency of oscillation is a function of the amplitude of motion and is limited by a maximum pitch rate of 15 deg per s attainable in the IAR facility. The largest amplitude of oscillation that can be tested depends on the mean angle of attack. The total angle cannot exceed 35 deg.

Unsteady data from the strain-gauged fin were digitally recorded at a sampling frequency of 100 Hz. The pressure transducer signals were recorded on FM tape and later digitized for analysis. The equivalent sampling rate was 80 kHz.

Boundary-layer transition trips were installed as in Ref. 1. Rows of epoxy cylinders (1.143-mm diam on 2.54-mm centers, 0.0508-mm high) were applied 10.16-mm behind the leading edges of the LEX, wings, intakes, vertical fins, and horizontal stabilators, on both surfaces. In addition, a ring of transition trips was applied around the nose, 10.16-mm behind the tip. Trips were also installed along the port and starboard sides of the forebody at approximately 36 deg to the underfuselage centerline. The trips were terminated approximately 558.8-mm from the nose, close to the engine inlet.

B. Fin Instrumentation

In this test the starboard fin was instrumented to measure unsteady pressures at 24 positions directly opposite to each other on each surface. Figure 1 shows the positions of the pressure transducers installed on the starboard vertical fin and their coordinates are given in Ref. 10. The construction and instrumentation of the fin are described in detail in Ref. 5.

The port fin was instrumented with strain gauges to provide accurate measurements of the normal force, root bending, and torsion moments. The bending and torsion effects have to be separated as much as possible to achieve the desired accuracy for load and moment measurements. This implies a careful choice of the configuration of the flexure and the placement of the strain gauges.

The design was based on a simple bending beam to transmit the load to the ground (fuselage), instrumented to measure bending moment at two positions and torsion moment about the beam axis. The final design is a balance between the need for moderate stress levels at the gauge locations and the desire to keep deflections within reasonable limits.

Figure 2 shows the plan view of the F/A-18 port fin. The locations of the beam flexure and the three strain gauge bridges are indicated. The beam was formed by wire cutting along the indicated line, which has a finished cut width of approximately 0.381 mm. The cut line was kept as close as possible

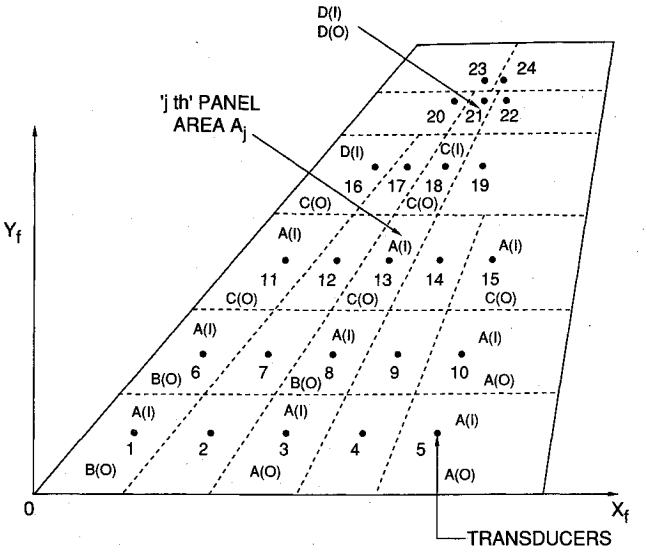

Fig. 1 Fin pressure transducer locations. A, B, C, and D denote the type of pressure signals illustrated in Fig. 14. I and O denote the inboard and outboard surfaces.

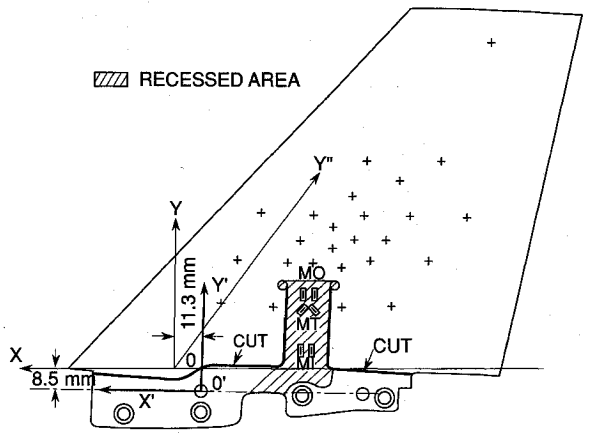

Fig. 2 Port fin instrumented with strain gauges. + Denotes loading points for calibration.

to the fin/fuselage junction, but was moved outboard into the fin surface in the vicinity of the cutout in the mounting attachment in order to retain adequate strength in that area.

High-resistance strain gauges were used to provide moderately high signal levels. The recessed areas containing the strain gauges and wiring were covered with RTV silicone compound contoured to the fin surface, with care being exercised to ensure that the compound did not fill the narrow cut line.

C. Port Fin Calibration

Performance was expected to be symmetrical for positive and negative loads and moments. This was confirmed from the data acquired during the loading cycle. The loads were applied at 25 positions and the data from loadings were used to define the calibration matrix. The load positions were concentrated mainly in the area of the fin corresponding to the anticipated region of the resultant force. However, some points located significantly outside this region were also provided.

The instrumented fin was a bending beam balance and measures the bending and torsion moments. It was convenient to define the calibration coefficients so that they related the measured strain gauge outputs to the overall forces and moments. The axis system and moment center to which the forces and moments apply were defined in Fig. 2 using the forward dowel location for fin mounting as the origin O′ of an orthogonal system of axes. The dimensions of all calibration

and check load points shown in the figure were referenced to this origin. The sign convention for the force and moments were normal force (NF) positive outward, root bending moment (BM) positive for tip deflected outward, and torsion moment (TM) positive when leading edge was twisted outward. This choice of the orthogonal axis system was made for convenience in measurements of the loading point coordinates. The axes used for presenting the bending and torsion moments results are shown in Fig. 2 by OX and OY″, respectively. The center O of the new coordinate system is shifted forward by 11.3 mm and outboard by 8.5 mm from the origin O′. The root bending axis remains parallel to the calibration axis (O′X′), but the torsion moment axis is swept back at an angle of 53 deg which corresponds to the $\frac{1}{4}$ chord line.

For each of the 25 calibrated loadings, the outputs from each of the strain gauge bridges (MI, MO, and MT in units of mV/V) were fitted to straight lines. The curve-fit coefficients together with the corresponding load point coordinates defined the coefficients of an overdetermined set of linear simultaneous equations. These are solved to yield the linear calibration matrix $[C]$ in the equation

$$\{\text{MI, MO, MT}\} = [C]\cdot\{\text{NF, BM, TM}\} \qquad (1)$$

The strain gauges are capable of measuring an estimated minimum of 96% of the normal force.

High-frequency unsteady load and moment analyses were not carried out from the strain gauge outputs. Instead, results from the summation of the pressure transducer signals on the starboard fin were used for statistical analysis and estimation of rms values. Wind-off resonant tests on the port fin showed the first bending and torsional frequencies to be 140 and 300 Hz, respectively.

III. Results and Discussion

A. Normal Force and Moments from Static Tests

Figure 3 shows the steady-state C_N on the vertical fin plotted against α from static wind-tunnel tests. The comparison between the strain gauge and pressure summation results is made at $M = 0.25$ and 0.8.

To obtain the normal force acting on the starboard fin, the difference in pressure between a transducer pair is multiplied by the panel area and summed over the total number of panels. This force is expressed in coefficient form by the following equation:

$$C_N = \sum_{j=1}^{24} (p_{Ij} - p_{Oj})A_j/qS \qquad (2)$$

The area A_j of the jth panel is shown in Fig. 1. It is assumed that the pressure measured by each transducer is constant throughout the panel. From Eq. (2), steady-state C_N and rms value C'_N can be computed.

The curves in Fig. 3 show that the strain gauge results are slightly above those from pressure measurements for $\alpha < 15$ deg and become smaller for $\alpha > 15$ deg. The difference decreases for increasing α. At $M = 0.8$, the results are practically the same when $\alpha \geq 27.5$ deg. Similar findings are also made for the bending and torsion moments. The good agreement of the results indicates that the pressure transducer locations and spacings used in previous measurements[5] are suitable for computing steady loads and moments on the vertical fin.

The effect of Mach number on the normal-force coefficient is shown in Fig. 4 for $M = 0.25$ ($q = 5.86$ kPa, $R_{e\bar{c}} = 1.6 \times 10^6$), $M = 0.6$ ($q = 27.44$ kPa, $R_{e\bar{c}} = 3.5 \times 10^6$), and $M = 0.8$ ($q = 40.81$ kPa, $R_{e\bar{c}} = 4.1 \times 10^6$). When $\alpha < 15$ deg, the values of C_N for the three Mach numbers are very close since the LEX vortices have little effect on the vertical fin pressures. Water-tunnel experiments[10] show that for α of approximately 15 deg, the vortex burst is very close to the vertical fin. In the range of 0 deg $< \alpha <$ 15 deg, the effect of the unburst vortex flow on the fin loads is small. The $M = 0.8$ results show a larger increase in C_N than the other two values of M. For $\alpha > 27.5$ deg, it is seen that the increase in C_N with α for $M = 0.6$ becomes very gradual, while for $M = 0.8$, C_N reaches a maximum at $\alpha = 27.5$ deg and decreases thereafter.

The bending and torsion moment coefficients C_B and C_T vary with α in a similar trend as that for C_N. Reference 11 describes Mach number effects and shows that they are more important in the range of α between 15 deg and approximately 30 deg. At $M = 0.8$, schlieren photography of the flowfield in the vicinity of the wing showed the presence of shock waves for values of α above 15 deg. These shock waves interact with the LEX vortices so as to alter the flowfield structure in the vicinity of the vertical fin. This will have an important effect on the loads and pressures on the fin.

B. Sinusoidal Pitching Motion

Figures 5 and 6 show the C_N and C_T variations with α at $M = 0.25$ for sinusoidal pitching motion. The results are time-averaged over 16 samples or 0.16 s. The frequency is 0.4 Hz and when expressed in terms of k, the value is approximately 0.001. At the frequencies and Mach numbers considered in this study, k is very close to zero.

Three values of the mean angle of attack $\alpha_0 = 10$, 20 and 27.5 deg are considered and the amplitude α_a is 5 deg. The static values of C_N and C_T from constant α runs are superimposed in the figures. It is seen that they lie approximately in between the oscillating model values. As noted in Ref. 9, during pitch-up motion there is a lag in the burst position of the LEX vortex. The vortex burst occurs at a point further downstream than the static position, resulting in an equivalent static condition with a smaller α.

During pitch-down motion, the opposite effect occurs. This is seen in Fig. 5 where the values of C_N are below and above the static values during a pitch-up and pitch-down motion, respectively. For the torsion moment C_T, Fig. 6 shows the

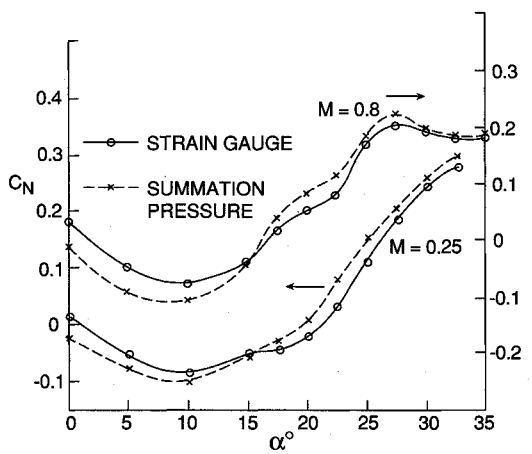

Fig. 3 Comparison of C_N from strain gauges and pressure summation. The arrow sign denotes the scale to be used for the two Mach numbers. C_N scale for $M = 0.8$ is shifted one unit upwards.

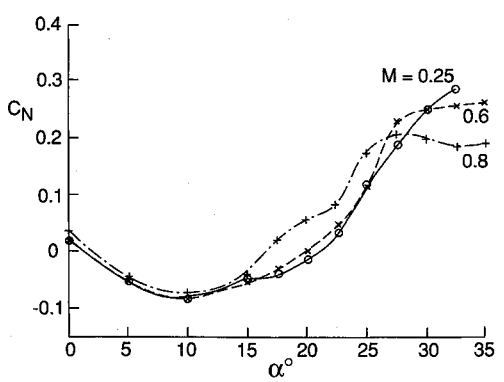

Fig. 4 Static variation of C_N with α.

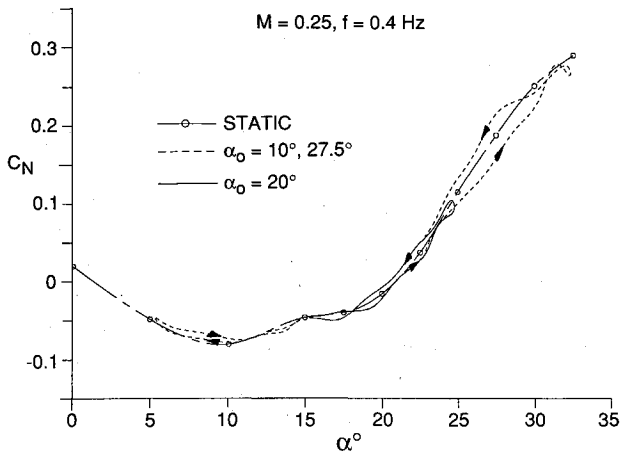

Fig. 5 Variation of C_N with α for pitch oscillations.

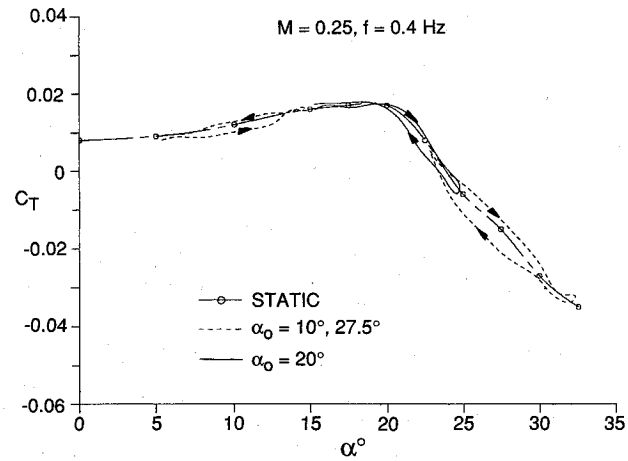

Fig. 6 Variation of C_T with α for pitch oscillations.

pitch-up and pitch-down values are above and below the static values, respectively. The absolute value is larger during the pitch-down motion. This is consistent with the lag effect due to delay in vortex burst. It is interesting to note that at the smallest value of $\alpha_0 = 10$ deg, the loads and moments measured during pitch-up and pitch-down motions do not follow the trend as that seen for the higher α_0 cases. In the range 5 deg $< \alpha <$ 15 deg, the flowfield is dominated by unburst vortex flow.

Mach number effects are shown in Figs. 7 and 8 for M = 0.25, 0.6, and 0.8. The mean angle of attack is 20 deg with $\alpha_a = 10$ deg and $f = 0.25$ Hz. Due to the limited number of runs performed at the higher Mach numbers, it was not possible to make comparisons at the highest frequency attainable in these tests which should show greater hysteresis effects. The shape and orientation of the loops are different as indicated by the static values given in Ref. 11.

C. Probability Density Function

The probability density of the normal force is shown in Fig. 9 for $M = 0.25$, $\alpha_0 = 15$ deg, $\alpha_a = 10$ deg, and $f = 0.25$ Hz. The shape is typical of those obtained for other values of M, α_0, α_a, and f. The density function resembles a gamma distribution given by the equation

$$p(x) = \frac{(3)^{1/4}\exp(-\sqrt{3}|x|/2\sigma)}{\sqrt{8\pi\sigma|x|}} \qquad (3)$$

This expression also approximates the probability densities for most of the transducers on the vertical fin except for some locations close to the lower right corner of the inboard surface. The probability density functions for transducers 3, 5, 8, and

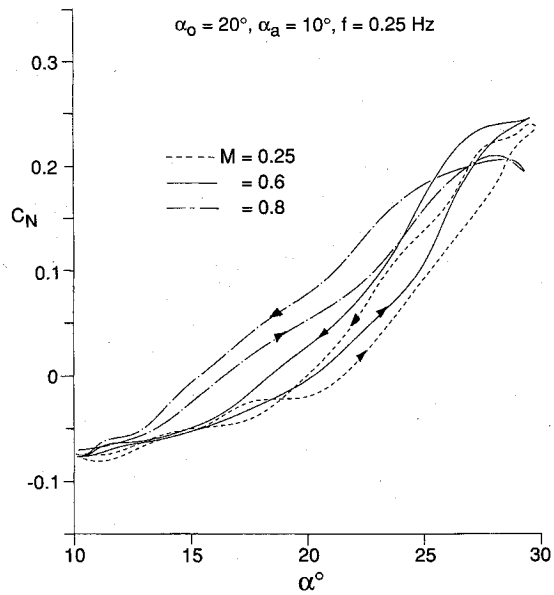

Fig. 7 Effect of Mach number on C_N.

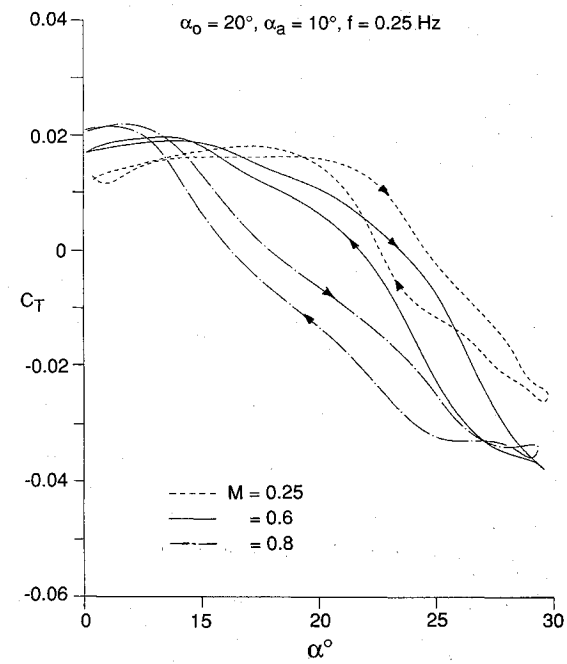

Fig. 8 Effect of Mach number on C_T.

10 (Fig. 1) on the inboard surface more closely resemble a Gaussian distribution.

The gamma distribution is often used in speech analysis and problems related to continuous waiting-time distributions. The distinct peak at zero is a result of pauses and low-level loadings on the vertical fin. A characteristic of the gamma distribution is the higher probability of encountering large amplitude fluctuations than in a Gaussian distribution. This type of probability distribution can be used to represent the nonstationary of the vertical fin load signals when the model is performing pitch oscillations. For static results at constant α, the load signal is statistically stationary. In Ref. 6, the probability densities of the fin normal force from static tests at $M = 0.6$ and α = 25, 30, and 35 deg are given. They show the normal force to behave very closely to a Gaussian process.

D. Time Variation of Normal Force

Figure 10 shows the variation of the fluctuating normal force coefficient on the vertical fin for the first three cycles of forced oscillations. The fluctuating C_N was obtained by subtracting

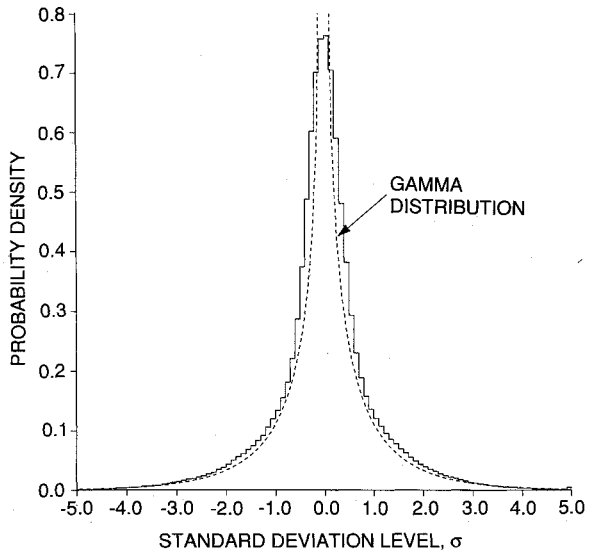

Fig. 9 Probability density of normal force at $M = 0.25$, $\alpha_0 = 15$ deg, $\alpha_a = 10$ deg, and $f = 0.25$ Hz.

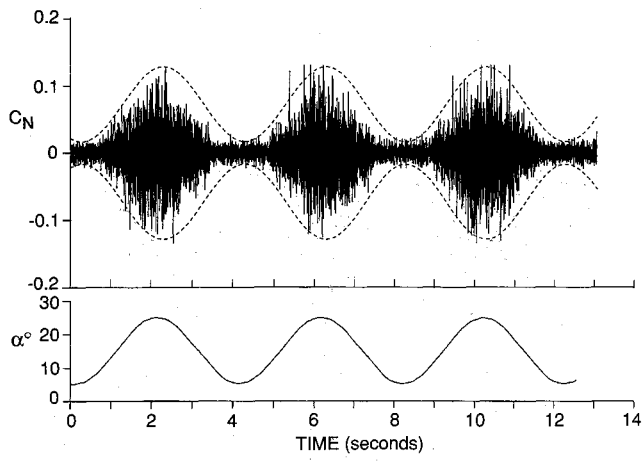

Fig. 10 Time variation of C_N at $M = 0.25$, $\alpha_0 = 15$ deg, $\alpha_a = 10$ deg, and $f = 0.25$ Hz.

the time-averaged mean from the instantaneous value of C_N. The test conditions were $M = 0.25$, $\alpha_0 = 15$ deg, $\alpha_a = 10$ deg, and $f = 0.25$ Hz. C_N was determined from summation of the pressure transducer outputs on the starboard fin using Eq. (2). The port fin data were not used since the frequency response was too low.

The envelope of the C_N curve is obtained by fitting a cosine function to the data. The equation of the envelope is determined from the equation

$$y = A|m + \cos(2\pi ft + \phi)| \tag{4}$$

where ϕ is the phase angle, A is the amplitude and m is a constant.

To determine ϕ, the time signal is divided into segments of 0.01 s and the rms values computed. The location of the maximum of the envelope is obtained from the maximum of the rms values of the signal. The average from the total number of cycles of data available, which in this case is six, is used to determine the average phase angle with reference to the angle of attack. For the particular example given in this article, the phase lag between the maximum fluctuations and the pitch angle is approximately 8 deg.

In Fig. 11 the time variation of the normal force obtained from the strain-gauged port fin is shown. The data was sampled at 100 Hz. After performing some smoothing of the data, the maximum C_N and minimum C_T can be located and they

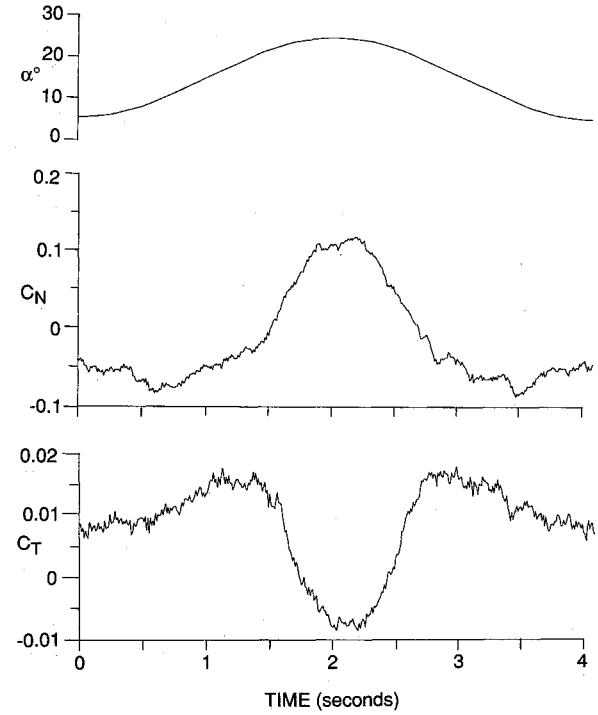

Fig. 11 Time variation of C_N and C_T from strain gauges at $M = 0.25$, $\alpha_0 = 15$ deg, $\alpha_a = 10$ deg, and $f = 0.25$ Hz.

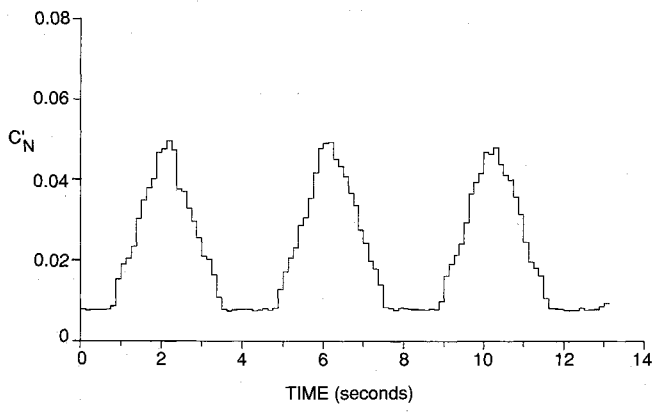

Fig. 12 Time variation of C'_N at $M = 0.25$, $\alpha_0 = 15$ deg, $\alpha_a = 10$ deg, and $f = 0.25$ Hz.

lag the pitch angle by approximately 0.1 s. When converted to angle, it is 9 deg. This is consistent with the value of ϕ evaluated from C_N in Fig. 10.

The value of A in Eq. (4) is determined from the requirement that the envelope encloses between 99.89 and 99.91% of the peaks. This is represented by the following equation:

$$99.89\% < P[|x| \leq a\sigma] < 99.91\% \tag{5}$$

where $P(x)$ is the probability. With A known, m is obtained such that $C_N = (m - 1)A$ will give the best fit to the experimental data when C_N is a minimum. For the case given in Fig. 10, $m = 1.3$.

In Fig. 10, the constant a for a probability of 99.91% is 4.89. For a gamma distribution, the value of a for $P(x) = 99.9\%$ is 5.517, while for a Gaussian distribution, $a = 3.1$. The results show that with the model performing low-frequency pitch oscillations, the vertical fin normal force fluctuations are statistically nonstationary. There is a higher probability of encountering large amplitude fluctuations than if the process is Gaussian.

The variation of the rms values with time is shown in Fig. 12. The C'_N is computed using a time segment of 0.125 s. The

change in C'_N with time does not follow a cosine function like the angle-of-attack curve. There is a pause time of approximately 1.4 s when the fluctuations are small and the rms values remain practically constant. This corresponds to the F/A-18 model position between 5–10 deg where the unburst LEX vortices have little effect on the vertical fin normal force fluctuations.

Figure 13 shows C'_N for the third oscillation cycle plotted against α. The filled and open circles denote the pitch-up and pitch-down motions, respectively. Superimposed on the data are the rms values obtained from static tests. At low α, the agreement between oscillating and static results is very good. As α increases, lower values of the rms fluctuations are detected for pitching motion. No significant difference between pitch-up and pitch-down values of C'_N within a cycle of oscillation is observed at this frequency.

E. Behavior of Pressure Signals

To investigate the behavior of the pressure-time signals on the vertical fin, the outputs from 12 transducers on each surface were recorded on FM tape and the later digitized for analysis. The transducers available for analysis are 1, 3, 5, 6, 8, 10, 11, 13, 15, 16, 18, and 21.

The different types of pressure fluctuations that are observed are given by the four representative signals in Fig. 14. Signal (A) is from transducer 5 on the outboard surface. This type of signal is mostly observed on the inboard surface. In this figure, C_p is obtained by subtracting the time-averaged value from the instantaneous C_p data. The curve behaves similarly to C_N shown in Fig. 10. The envelope enclosing 99.9% of the peak fluctuations can be represented by a cosine function using Eq. (4). The corresponding C'_p vs time and α curves are shown in Figs. 15(A) and 16(A). Again a time segment of 0.125 s is used to evaluate rms values. The solid lines in Fig. 16 are the rms values determined from static tests.

The second type of signal is found at only three locations on the outboard surface for this particular example. Fig. 14(B) shows the pressure trace at transducer 1 on the outboard surface. The other transducers with similar time signal are transducer 6 and 8 on the same surface. The envelope for C_p has a frequency twice that of the model oscillation frequency. This type of behavior occurs when C'_p vs α behaves as in Fig. 16(B) where a peak occurs at moderate values of α. For certain combinations of α_0 and α_a, the maximum is crossed twice in one cycle of oscillation, resulting in the double peaks shown in Fig. 15(B).

The next type of signal is shown in Fig. 14(C) and is found mostly on the outboard surface for distances greater than 50% span from the fin/fuselage junction. The signal shown is from transducer 16 on the outboard surface. The C'_p vs α curve in Fig. 16(C) is similar to Fig. 16(B), except that the peak moved

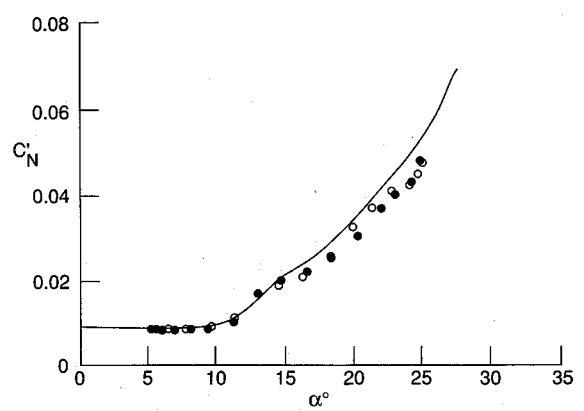

Fig. 13 Variation of C'_N with α at $M = 0.25$, $\alpha_0 = 15$ deg, $\alpha_a = 10$ deg, and $f = 0.25$ Hz. ● Pitch-up motion, ○ pitch-down motion, —— static values.

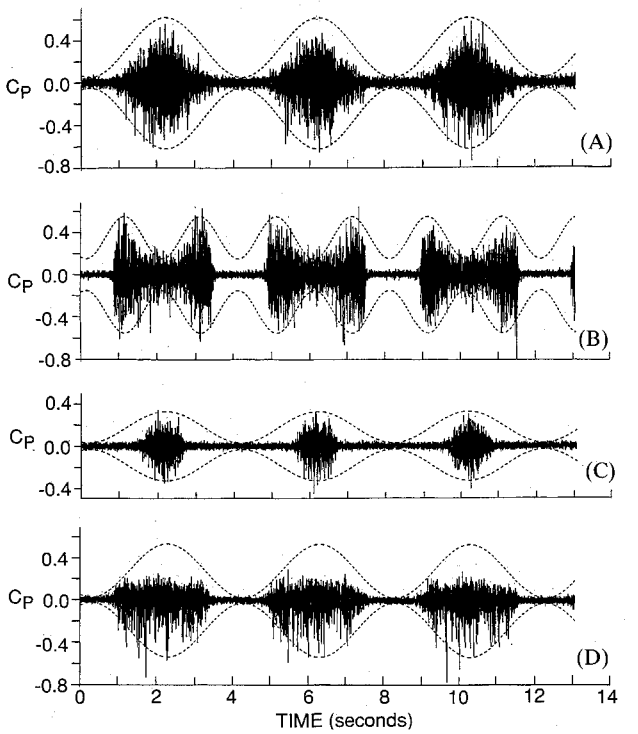

Fig. 14 Time variation of C_p at $M = 0.25$, $\alpha_0 = 15$ deg, $\alpha_a = 10$ deg, and $f = 0.25$ Hz.

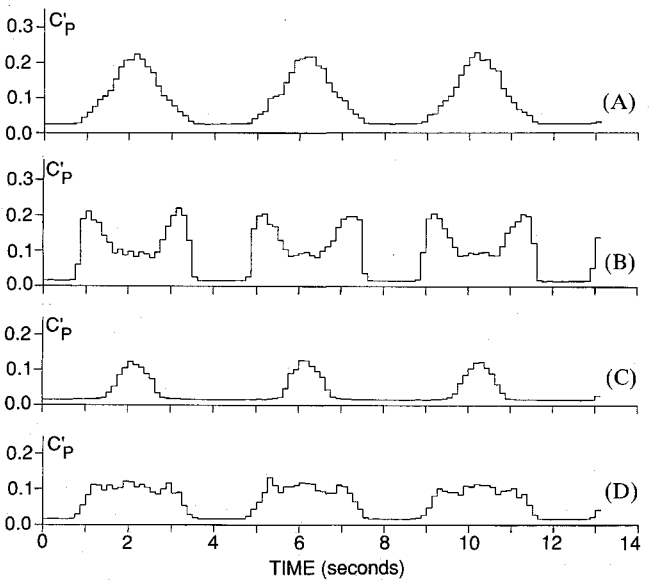

Fig. 15 Time variation of C'_p at $M = 0.25$, $\alpha_0 = 15$ deg, $\alpha_a = 10$ deg, and $f = 0.25$ Hz.

to a larger value of α. For combinations of α_0 and α_a such that the peak value is not crossed, as in this example, C'_p remains very small and constant for most of the oscillation cycle. The time series has a long pause before the magnitude of the pressure fluctuations becomes significant. In this example, the pause is about 2.8 s. From Fig. 16(C), the angle at which C'_p starts to increase is approximately 21 deg. Near the fin/fuselage junction, pressure fluctuations begin to increase rapidly for $\alpha > 15$ deg. Figure 16(C) shows that for distances greater than 50% span, some of the outboard transducers will not experience any large pressure fluctuations until α reaches a value larger than 15 deg. The only transducer on the inboard surface that exhibits this type of behavior is transducer 18.

The last type of signal detected is shown in Fig. 14(D) for transducer 16 on the inboard surface. In this case, there are

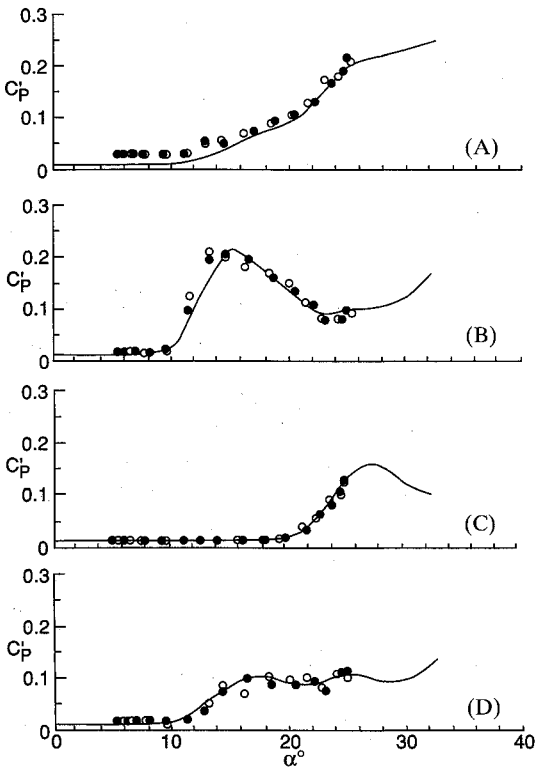

Fig. 16 Variation of C_p' with α at $M = 0.25$, $\alpha_0 = 15$ deg, $\alpha_a = 10$ deg, and $f = 0.25$ Hz. ● Pitch-up motion, ○ pitch-down motion, —— static values.

more negative than positive peaks. The rms values in Fig. 15(D) show a fairly constant value for a time interval of approximately 2 s. The C_p' vs α curve [Fig. 16(D)] shows there is a gradual increase from 10 to 15 deg. When α exceeds 15 deg, the rms values are fairly uniform. This type of behavior in the pressure fluctuations occurs mostly near the fin tip. Figure 1 summarizes the type of pressure signals found on the inboard and outboard surfaces for the example discussed.

The phase angles determined from Eq. (4) for both sets of transducers on the inboard and outboard surfaces are fairly close to the value for C_N. They are mostly within 3 deg of the C_N phase angle. Only two transducers close to the trailing edge of the fin on the inboard surface at locations 10 and 15 show a larger difference of approximately 8 deg. These two transducers are nearly in phase with the pitch motion.

IV. Conclusions

Comparisons of steady normal force, bending and torsion moments on an F/A-18 vertical fin determined from pressure summation and strain gauge measurements, show good agreement. The transducer locations and spacings used in previous measurements are shown to be suitable for computing static loads and moments on the vertical fin.

For static tests at different Mach numbers, the fin C_N, C_B, and C_T variations with α show that at angles of attack less than 15 deg, the results are very close. In the range 0 deg $< \alpha <$ 15 deg, the effect of the unburst LEX vortices on the fin loads is small. The $M = 0.8$ results show a larger increase in force and moments with α than at $M = 0.25$ and 0.6. At $M = 0.8$, schlieren photography shows the presence of shock waves and transonic effects become important.

When the F/A-18 model is oscillating in pitch, the lag effect of vortex burst on fin loadings is important even at very low frequencies. The peak normal force is found to lag the pitch angle by approximately 9 deg or 0.1 s in the example given for $M = 0.25$ and $f = 0.25$ Hz. There was insufficient data to provide results showing frequency and Mach number effects on the phase relation.

The characteristics of the pressure fluctuations are discussed and four possible types of pressure behavior are illustrated.

The probability density function of the fin load at low-pitch frequencies shows that it can be represented by a gamma distribution. Most of the pressures on the fin surfaces can also be approximated by the gamma distribution.

Acknowledgments

The authors are indebted to the Institute for Aerospace Research for support of the high angle-of-attack research project. The Department of National Defence provided funds for the instrumentation of the F/A-18 wind-tunnel model. They wish to thank R. Galway, F. Ellis, D. Brown, Z. Ben-Neticha, and N. Valerio for their valuable assistance.

References

[1]Erickson, G. E., Hall, R. M., Banks, D. W., Del Frate, J. H., Schreiner, J. A., Hanley, R. J., and Pulley, C. T., "Experimental Investigation of the F/A-18 Vortex Flows at Subsonic Through Transonic Speeds, Invited Paper," AIAA Paper 89-2222, AIAA 7th Applied Aerodynamics Conf., Seattle, WA, July 31–Aug. 2, 1989.

[2]Fisher, D. F., Del Frate, J. H., and Zuniga, F. A., "Summary of In-Flight Flow Visualization Obtained from the NASA High Alpha Research Vehicle," NASA TM-101734, Jan. 1991.

[3]Shah, G. H., Grafton, S. B., Guynn, M. D. Brandon, J. M., Dansberry, B. E., and Patel, S. R., "Effect of Vortex Flow Characteristics on Tail Buffet and High-Angle-of-Attack Aerodynamics of a Twin-Tail Fighter Configuration," High-Angle-of-Attack Technology Conf., NASA Langley Research Center, Hampton, VA, Oct. 30–Nov. 1, 1990.

[4]Martin, C. A., Glaister, M. K., MacLaren, L. D., Meyn, L. A., and Ross, J., "F/A-18 1/9th Scale Model Tail Buffet Measurements," Aeronautical Research Lab., ARL-FLIGHT-MECH-R-188, AR-006-149, Melbourne, Australia, June 1991.

[5]Lee, B. H. K., and Brown, D., "Wind Tunnel Studies of F/A-18 Tail Buffet," *Journal of Aircraft*, Vol. 29, No. 1, 1992, pp. 146–152.

[6]Lee, B. H. K., and Tang, F. C., "Buffet Load Measurements on an F/A-18 Vertical Fin at High-Angle-of-Attack," AIAA Dynamics Specialists Conf., AIAA Paper 92-2127, Dallas, TX, April 16–17, 1992.

[7]Lee, B. H. K., Brown, D., Tang, F. C., and Plosenski, M., "Flowfield in the Vicinity of the F/A-18 Vertical Fin at High-Angle-of-Attack," *Journal of Aircraft* (to be published).

[8]Lee, B. H. K., and Dunlavy, S., "Statistical Prediction of Maximum Buffet Loads on the F/A-18 Vertical Fin," *Journal of Aircraft*, Vol. 29, No. 4, 1992, pp. 734–736.

[9]Hebbar, S. K., and Platzer, M. F., "A Water Tunnel Investigation of the Effects of Pitch Rate and Yaw on LEX Generated Vortices on an F/A-18 Fighter Aircraft Model," AIAA 29th Aerospace Sciences Meeting, AIAA Paper 91-0280, Reno, NV, Jan. 1991.

[10]Lee, B. H. K., Brown, D., Zgela, M., and Poirel, D., "Wind Tunnel Investigation and Flight Tests of Tail Buffet on the CF-18 Aircraft," *AGARD Conference Proceedings No. 483*, Sept. 1990, pp. 1.1–1.26.

[11]Lee, B. H. K., and Tang, F. C., "Unsteady Pressure and Load Measurements on an F/A-18 Vertical Fin at High-Angle-of-Attack," AIAA 10th Applied Aerodynamics Conf., AIAA Paper 92-2675, Palo Alto, CA, June 22–24, 1992.